Charge carrier localization in La1-xSrxMnO3 investigated by AC conductivity measurements

A. Seeger, Peter Lunkenheimer, Joachim Hemberger, A. A. Mukhin, V. Yu. Ivanov, A. M. Balbashov, Alois Loidl

Seeger, A., Peter Lunkenheimer, Joachim Hemberger, A. A. Mukhin, V. Yu. Ivanov, A. M. Balbashov, and Alois Loidl. 1999. "Charge carrier localization in La1-xSrxMnO3 investigated by AC conductivity measurements." *Journal of Physics: Condensed Matter* 11 (16): 3273–90. https://doi.org/10.1088/0953-8984/11/16/009.

Charge carrier localization in $La_{1-x}Sr_xMnO_3$ investigated by ac conductivity measurements

A Seeger†, P Lunkenheimer†, J Hemberger†, A A Mukhin‡, V Yu Ivanov‡,
A M Balbashov§ and A Loidl†

† Experimentalphysik V, Universität Augsburg, 86135 Augsburg, Germany
‡ General Physics Institute of the Russian Academy of Sciences, 117942 Moscow, Russia
§ Moscow Power Engineering Institute, 105835 Moscow, Russia

Abstract. We have investigated the complex ac conductivity of $La_{1-x}Sr_xMnO_3$ for $0 \leqslant x \leqslant 0.2$, temperatures $15\ K \leqslant T \leqslant 300\ K$ and frequencies $20\ Hz \leqslant \nu \leqslant 1.8\ GHz$. In addition, results from dc measurements are presented. From the frequency dependence of the complex conductivity we find hopping of Anderson-localized charge carriers as the dominant transport process in certain temperature and composition ranges. We deduce that, while Anderson localization is not the driving mechanism for the metal–insulator transition observed in this compound, it is responsible for the high-resistivity regions observed at low doping levels and low temperatures. The results indicate a polaronic nature of the charge carriers. From the temperature dependence of the ac conductivity and the magnetic permeability, deduced in the skin-effect-dominated regime, various phase transition temperatures have been determined.

1. Introduction

For almost half a century, starting with the pioneering work of Jonker and van Santen [1], it has been well known that the manganite perovskites $L_{1-x}A_xMnO_3$, with L a trivalent lanthanide cation and A a divalent cation, show many puzzling properties [2]. Early theoretical work [3] established the double-exchange (DE) transport mechanism as an explanation of the close relationship between magnetic and transport properties in these materials. In the past decade some of these materials ($La_{1-x}A_xMnO_3$, A = Sr, Ca, Ba, Ni, Mg) played an important role in the development of solid oxygen fuel cells (SOFCs) [4]. Their high electrocatalytic activity in connection with good chemical compatibility with the electrolyte material and a relatively high conductivity in oxidizing atmospheres make them well suited as cathode material in SOFCs. However, the overwhelming interest in these materials which has led to a vast number of publications in recent years is due to the exceptionally high magnetoresistance found for certain composition ranges [5]. This property, commonly termed `colossal magnetoresistance' (CMR) opens up a large field of applications, e.g., as materials for magnetic recording devices. But even apart from their possible applications these materials are very attractive, mainly due to the presence of many competing interactions (superexchange, double exchange, charge ordering and Jahn–Teller effect). This leads to very rich phase diagrams which include a variety of structural and magnetic phases and the presence of metal–insulator (MI) transitions. However, despite the long history of investigation of these materials, their phase diagrams are not completely clarified yet and still a matter of discussion [6–10].

A main goal of current investigations on the perovskite manganites is the clarification of their transport mechanism including the observed MI transitions. The theoretical work of Millis *et al* [11] led to the notion that, aside from the DE, there must be additional mechanisms affecting the charge transport. They considered the strong electron–phonon coupling due to the Jahn–Teller (JT) effect present at the oxygen octahedra surrounding the Mn^{3+} sites. Doping with divalent A^{2+} cations is believed to generate Mn^{4+} ions which are not subjected to the JT effect. For $x < 0.5$ this corresponds to the formation of a polaron at the Mn^{4+} site. Indeed, since then many investigations [12] have confirmed the importance of electron–phonon interactions in these materials. In the picture of Millis *et al*, the JT effect leads to the opening of a gap at the Fermi level which, together with the DE, gives at least a qualitative description of the experimental observations. However, also alternative explanations have been proposed and the mechanism leading to the observed transport properties and the MI transition is still a matter of controversy. E.g., in addition to polaronic mechanisms, charge ordering seems to play an important role in these materials [9]. Also it was proposed [13] that these materials fall in the category of charge transfer insulators in the classification scheme of Zaanen *et al* [14]. As the DE does not consider the oxygen p-like bands (the DE-induced MI transition resembles a Mott–Hubbard transition) modifications of the DE may be necessary, that could be sufficient to explain the experimental findings without invoking polaron contributions. The effects described so far have in common that the transport properties are essentially explained within a band conducting picture. However, it seems clear that also disorder must play an important role in these doped materials [15]. Disorder can lead to Anderson localization of charge carriers which may be responsible, at least partly, for the semiconducting regions and the MI transitions observed in the perovskite manganites. To check for the presence of Anderson localization and investigate its importance in the x–T phase diagram of the perovskite manganites is the aim of the present work. In certain concentration ranges, $La_{1-x}Sr_xMnO_3$ exhibits two semiconducting regions divided by a small metal-like region (i.e. with $\partial\rho_{dc}/\partial T > 0$, ρ_{dc} the dc resistivity) extending some ten degrees below the magnetic ordering temperature, T_c [8]. We want to clarify, whether Anderson localization plays a role in these semiconducting regions. Also information on the type of charge carriers will be obtained. Finally, we will try to obtain information on the presence and nature of the phase transitions in this material.

The measurement of the complex frequency-dependent conductivity is an ideal tool to investigate charge transport by hopping of Anderson-localized charge carriers (polarons or others) [16]. Besides the determination of the presence of Anderson localization it can provide information concerning the nature of the charge carriers and transport processes. In the present work we report measurements of the dc and the complex ac conductivity and resistivity of $La_{1-x}Sr_xMnO_3$ which probably is the most thoroughly investigated CMR system. For the most recent phase diagrams of this system the reader is referred to the literature [6–10]. The measurements have been performed at frequencies $20\ \mathrm{Hz} \leqslant \nu \leqslant 1.8\ \mathrm{GHz}$ and temperatures $1.5\ \mathrm{K} \leqslant T \leqslant 300\ \mathrm{K}$. The compositions investigated were $x = 0$, 0.05, 0.075, 0.1, 0.125, 0.15, 0.175 and 0.2 thereby covering the most interesting phases exhibiting the CMR and MI transitions. We will restrict the detailed discussion of the results to $x = 0$, 0.15 and 0.175, the other samples showing similar behaviour.

2. Experimental details

Single crystals of $La_{1-x}Sr_xMnO_3$ ($x = 0, 0.05, 0.075, 0.1, 0.125, 0.15, 0.175, 0.2$) were grown by the floating zone method with radiation heating. Raw La_2O_3, $SrCO_3$ and Mn_3O_4 chemicals of a high purity (not less 99.99%) were used for ceramic rod preparation. Some excess of

Mn_3O_4 concentration ($\sim$0.5 at.%) was used in order to compensate an Mn loss due to an evaporation from the melt in the floating zone melting. The initial synthesis of composition was provided by annealing of mixed chemical powder at temperature about 1200 °C for 24 h. After pressing of feed rods they undergo sintering at 1350 °C for 24 h. The single crystals of $x \leqslant 0.075$ compositions were grown in an Ar atmosphere while for $x > 0.075$ an air atmosphere was used. The typical crystal growth speed was 7–10 mm h^{-1} for a rotation speed of the crystal and feed rod $\sim$60 r min^{-1}. The typical growth direction was [110]. In order to obtain crack free crystals they were annealed at a temperature of about 1300 °C.

X-ray powder diffraction measurements showed that grown materials were of single phase. The rocking curves from the (110) plane have the halfwidth in the range 30–80″. The misorientation of sub-blocks in the cross-section of the crystal did not exceed 1° with respect to the [110] direction. Two dimensional x-ray TV topography of the crystals has revealed a twin structure for compositions $0 \leqslant x \leqslant 0.175$. The minimal twinning was observed for $x = 0.05$. For electrical contacts two surfaces of the crystal have been covered with silver paint. Due to the twinning of the crystals, the direction of the electric field with respect to the crystallographic directions was not well defined.

The measurements of the dc conductivity were performed using standard four-point techniques. For regions of extremely high resistance ($R > 10^9\ \Omega$, the sample resistance being much larger that the contact resistance) a two-point technique employing an electrometer was used. For measurements of the ac electrical properties in the low-frequency region, 20 Hz $\leqslant \nu \leqslant$ 1 MHz, an autobalance bridge (HP4284 LCR-meter) was used. For samples with relatively high conductivity ($x \geqslant 0.175$) the application of the four-point technique was possible in order to avoid contact contributions. For the lower concentrations the two-point technique was mandatory due to the restrictions of the LCR-meter. To carry out temperature dependent measurements, the samples were mounted on the cold plate of a closed cycle refrigerator or in a ^{4}He cryostat and connected to the bridge by four coaxial cables in order to avoid cable contributions.

For the measurements in the radiofrequency range a reflectometric technique was employed. The sample was mounted at the end of a coaxial air line, connecting the inner and outer conductors [17]. The complex reflection coefficient, Γ, of this assembly has been recorded using HP4191 and HP4291 impedance analysers for frequencies 1 MHz $\leqslant \nu \leqslant$ 1 GHz and 1 MHz $\leqslant \nu \leqslant$ 1.8 GHz, respectively. The complex conductivity or resistivity can be calculated from Γ after proper calibration using three standard samples to eliminate the influence of the coaxial line. The influence of the sample holder is mainly given by an additive inductance contribution. For cooling, the end of the coaxial line has either been connected to the cold head of a closed cycle refrigerator or brought into a ^{4}He cryostat. Reflectometric methods require two-point contact configurations.

3. Results and discussion

3.1. Dc transport

Figure 1 shows the temperature-dependent dc resistivity of all samples investigated. The curves agree well with the results reported in the literature [8, 10] extending them to higher values of the resistivity. In the semiconducting regions of the phase diagrams, the CMR manganites show marked deviations from thermally activated behaviour of the temperature-dependent dc resistivity. In some publications [15, 18] these deviations have been described in the framework of the variable range hopping (VRH) model [19]. Figure 2 shows the temperature dependence of the dc resistivity for $x = 0$ and $x = 0.125$ in Arrhenius, $\log_{10} \rho_{dc}$–$1/T^{1/2}$ and $1/T^{1/4}$

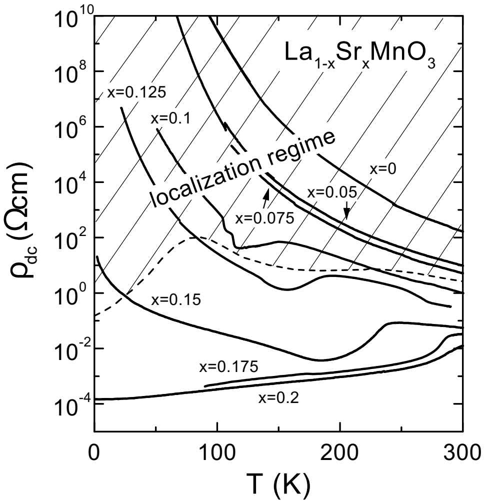

Figure 1. Temperature dependence of the dc resistivity for various Sr concentrations x. The curve for $x = 0.175$ was measured at 240 Hz. The hatched area indicates the Anderson localization regime as deduced from the ac measurements.

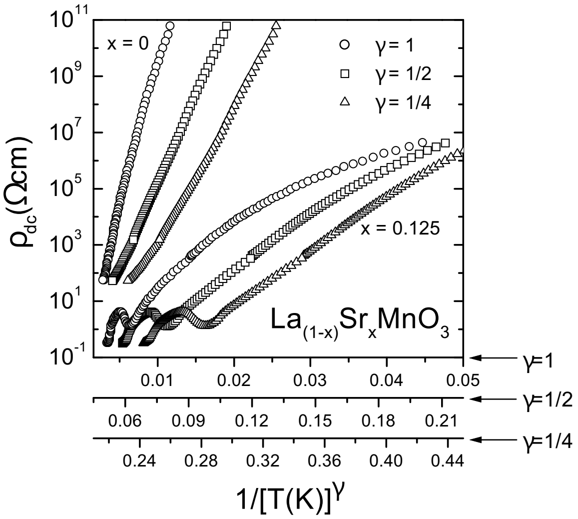

Figure 2. Temperature dependence of the dc resistivity for $x = 0$ and $x = 0.125$. The data are shown in three different representations, namely against $1/T$, $1/T^{1/2}$ and $1/T^{1/3}$.

representations. For both materials $\rho_{dc}(T)$ deviates from thermally activated behaviour. The alternative representations take account of a behaviour $\rho_{dc} = \rho_0 \exp[(T_0/T)^{1/\gamma}]$ with $\gamma = 2$ or 4 which is indicative of charge transport by tunnelling of electrons or holes. In the VRH model [19], $\gamma = 4$ is predicted for isotropic charge transport. Values of $\gamma = 3$ and 2 arise for VRH conduction in two and one dimensions, respectively [19, 20]. As pointed out by Efros and Shklovskii [21], an alternative explanation for $\gamma = 2$ can also be given when in Mott's model for three dimensions the Coulomb interaction between the charge carriers is taken into account.

For $x = 0$ an almost straight line is obtained for $\log_{10} \rho_{dc}$ against $1/T^{1/2}$ in the whole accessible temperature range of $85 \text{ K} < T < 300 \text{ K}$ (at lower temperatures ρ_{dc} is outside the limit of resolution of the experimental set-up). However, the deviations from a behaviour with $\gamma = 1/3$ (not shown) and $\gamma = 1/4$ are only small. Similar results were obtained for $x = 0.05$ and 0.075. For $x = 0.125$ the most convincing result (straight line) is observed for $\log_{10} \rho_{dc}$ against $1/T^{1/4}$ at temperatures $25 \text{ K} < T < 140 \text{ K}$, which is typical for three-dimensional VRH. In accord with previous reports [8], at higher temperatures $\rho_{dc}(T)$ increases, resembling metallic behaviour before resuming the semiconducting characteristics above 190 K. The $x = 0.1$ compound behaves in a similar way. For $x = 0.15$ none of the representations of figure 2 is able to describe $\rho_{dc}(T)$ satisfactorily. This compound is relatively close to the metal semiconductor transition which probably obscures the pure semiconducting response. Also phase separation may play a role in this compound [7, 22]. Concerning the $\gamma = 2$ behaviour for the low-doped compounds and a possible interpretation within the Efros–Shklovskii framework [21], at first glance it seems unlikely that, despite the smaller charge carrier density, there are stronger charge carrier interactions than in the higher-doped samples. However, it was argued that for samples that are close to the Anderson transition, indeed a transition from $\gamma = 2$ to $\gamma = 4$ behaviour could occur [23]. But also a different dimensionality of the transport depending on doping cannot be excluded, e.g. perpendicular to the planes for low doping and within the planes for higher doping. Overall, the difference of the plots with $\gamma = 1/2$ and 1/4 is rather small and a definite conclusion concerning the dimensionality of transport or the importance of charge carrier correlations cannot be drawn from these data alone. A problem arising in the analysis within the VRH framework is that DE and VRH are rather different transport mechanisms and it is not clear how they mix up, i.e. how, e.g., the Hund coupling modifies the VRH or how the tunnelling would modify the DE.

In summary, already the dc results show that these compounds are not simple band semiconductors but Anderson localization plays an important role in their transport processes. VRH gives a good description of $\rho_{dc}(T)$ for all compositions $x \leqslant 0.125$. From the dc results alone it is difficult to decide in what temperature ranges the localization prevails over band conduction as the differences between VRH and thermally activated behaviour are rather subtle. In this respect more precise information can be expected from the ac measurements.

3.2. Contributions to the complex conductivity

In this paragraph we will give a short overview of the phenomena affecting the complex conductivity of semiconducting and metallic materials in the relevant frequency range. Anderson-localized charge carriers contribute to the conductivity by hopping processes. Independent of the nature of charge carriers, hopping leads to an increase of real and imaginary parts of the complex conductivity $\sigma^* = \sigma' - \mathrm{i}\sigma''$ with frequency ν. This behaviour can be parametrized using a power law with exponent $s < 1$ [24]. By adding a term accounting for the dc conductivity, σ_{dc}, and for the high-frequency limit of the dielectric constant, ε_∞, one obtains:

$$\sigma' = \sigma_{dc} + \sigma_0 \nu^s \tag{1a}$$

$$\sigma'' = \tan(s\pi/2)\sigma_0 \nu^s + \varepsilon_\infty \varepsilon_0 2\pi \nu \tag{1b}$$

a behaviour usually termed `universal dielectric response' (UDR) [24]. When measuring in a sufficiently broad frequency range it is often seen that for low temperatures the ν^s power law of $\sigma'(\nu)$ crosses over to a linear increase, $\sigma' \sim \nu$ [24, 25]. This behaviour is often observed when measuring at sufficiently high frequencies in a variety of materials [24, 25] and quite recently was termed `second universality' (SU) [25]. There is no generally accepted microscopic picture

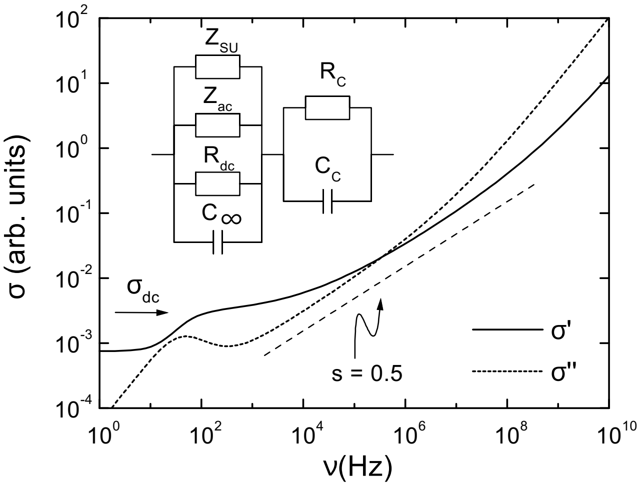

Figure 3. Typical behaviour of real and imaginary part of the conductivity resulting from the equivalent circuit shown as inset. The circuit takes account of contact contributions (R_c, C_c), UDR (R_{dc}, Z_{ac}, C_∞) and SU (Z_{SU}). For s a value of 0.5 was chosen; a `pure' ν^s power law is indicated in the figure.

for the origin of the SU. A vast number of theoretical approaches was employed to deduce the UDR behaviour from the microscopic transport properties of various classes of materials. Processes involving hopping over, or tunnelling through, an energy barrier separating different localized states have been considered for various kinds of charge carrier [16, 24]. However, common to all theories is the result that $\sigma' \sim \nu^s$, which holds true at least in a limited frequency range. Important information concerning the microscopic hopping process can be gained from the absolute value and the temperature dependence of the frequency exponent s.

The measurement of the ac response at high frequencies usually involves the use of two-point techniques. Therefore the contacts between electrode and sample material may contribute to the overall electric response. This is especially true for semiconducting samples where a surface layer of low carrier concentration may form due to the presence of Schottky diodes at the semiconductor metal contact. Other possible reasons are an ill defined stoichiometry or simply dirt at the surface. These contributions often can be described by an equivalent circuit consisting of the contact resistance R_c parallel to the contact capacitance C_c. This circuit in series with the frequency and temperature dependent sample impedance, given by the UDR and the SU, leads to the overall equivalent circuit shown in figure 3. Here R_{dc}, Z_{ac}, Z_{SU} and C_∞ take account of the σ_{dc}, ν^s, ν^1 and ε_∞ contributions, respectively. In figure 3, a typical behaviour for $\sigma'(\nu)$ and $\sigma''(\nu)$ resulting from this circuit is shown in double logarithmic representation. At low frequencies $\sigma'(\nu)$ exhibits a steplike increase which can be ascribed to a successive bridging of the contact resistance by the contact capacitance acting like a short at high frequencies. Correspondingly a peak shows up in $\sigma''(\nu)$. Above 10^3 Hz, for the parameters chosen, the response is dominated by the intrinsic contributions, i.e. UDR and SU. $\sigma'(\nu)$ exhibits a plateau corresponding to the dc contribution σ_{dc} and above about 10^5 Hz it starts to approach the power law $\sigma' \sim \nu^s$ (here $s = 0.5$ has been chosen). For higher frequencies the SU response, $\sigma' \sim \nu$ starts to dominate. In $\sigma''(\nu)$, due to the missing dc contribution, the ν^s power law is reached already at about 10^3 Hz while for higher frequencies the slope of $\sigma''(\nu)$ increases approaching a linear behaviour due to the ε_∞ contribution, see equation (1b). At low temperatures the contact contribution often shifts out of the frequency window leaving the intrinsic sample response. This is due to the semiconducting behaviour of the contact resistance, i.e. the characteristic time $\tau_c = R_c C_c$ of the contact RC-circuit increasing with decreasing temperature.

Many more contributions to the complex conductivity are possible. In dielectric materials often relaxation processes show up which can be attributed to the reorientation of dipolar degrees of freedom or to the hopping of charged particles in double- (or multiple-) well potentials [26]. Especially for materials with high conductivity, inductive components may arise from the electrical connections or the sample itself. They can be taken into account by assuming an equivalent circuit consisting of sample resistance connected in series to an inductivity while capacitive elements as C_∞ or contacts usually play no important role for high-conductivity materials. Therefore for more metallic materials the plotting of the complex resistivity instead of conductivity is the more `natural' form of representation [24] leading to a simpler behaviour. For metallic materials, at high frequencies the skin effect can cause a reduction of the current-carrying cross section and thereby to an increase of the measured sample resistance. The skin depth $\delta = [\rho_{dc}/(\tau\mu\mu_0\nu)]^{1/2}$, with μ_0 the permeability constant, depends on the magnetic permeability μ of the material investigated. Therefore a change of frequency dependence can be expected when the material is driven across a magnetic phase transition.

In this context it should be mentioned that throughout this article the presented conductivity and resistivity plots contain the data calculated using the geometrical factors only, i.e. $\sigma = Gd/A$ and $\rho = RA/d$ (G the conductance, R the resistance, d the thickness and A the cross section of the sample). Therefore, if skin effect or contacts affect the sample response, the plotted results do not correspond to the intrinsic σ or ρ.

3.3. *LaMnO$_3$*

Figure 4 shows the temperature dependence of the real part of the complex conductivity of LaMnO$_3$ for various frequencies, measured in the two-point technique. In addition, the dc conductivity (four-point technique for $T > 120$ K) is shown. Marked deviations from the dc curve are seen which extend up to some decades for the lowest temperatures investigated. At low temperatures the ac curves are located at higher values than the dc curve while at high temperatures this behaviour is partly reversed. As demonstrated in figure 3, the latter behaviour can be attributed to contact effects. E.g. at 300 K, only at 190 GHz the intrinsic dc conductivity is detected while for lower frequencies contact contributions dominate. The upward deviations from the dc curve can be attributed to the ν^s contribution in equation (1a) and/or the SU contribution. In addition, at low temperatures a peak is superimposed. Its position shifts to higher temperatures with frequency, indicative of a relaxation process. For LaMnO$_3$ a transition into an antiferromagnetically ordered state is reported at $T_N \approx 140$ K. Neither the dc nor the ac conductivity seem to be affected by this transition.

Figure 5(a) shows the same data in the frequency domain with temperature as parameter. In figure 5(b) the imaginary part is plotted. The spectra show the typical features seen in figure 3. In addition, the relaxation shows up in $\sigma'(\nu)$ as a shoulder near 10 MHz, superimposed on the low-temperature curves. For temperatures $T < 140$ K the contact contribution is completely shifted out of the frequency window. For high frequencies, $\sigma'(\nu)$ approaches a slope of 1 (dashed line in figure 5(a)) which clearly demonstrates the presence of an SU contribution. At 100 K also the dc contribution is shifted out of the frequency window and a ν^s increase is nicely seen preceding the SU region. These findings evidence the presence of Anderson-localized charge carriers and charge transport by hopping in this material. The lines in figure 5 are fits assuming the equivalent circuit of figure 3 with the UDR, equation (1a, b) and SU

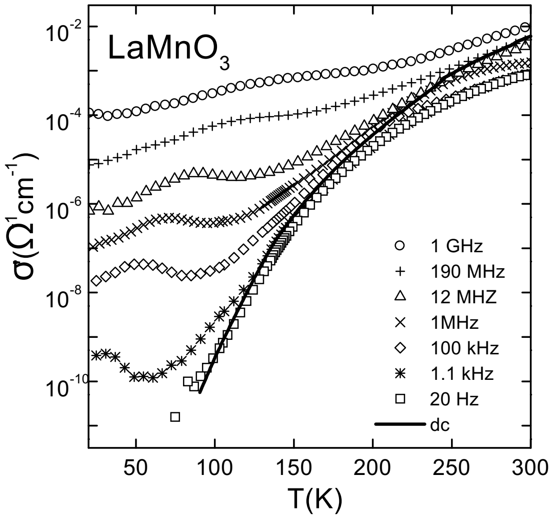

Figure 4. Temperature-dependent real part of the conductivity for $x = 0$ at various frequencies. In addition the dc conductivity is shown as a solid line.

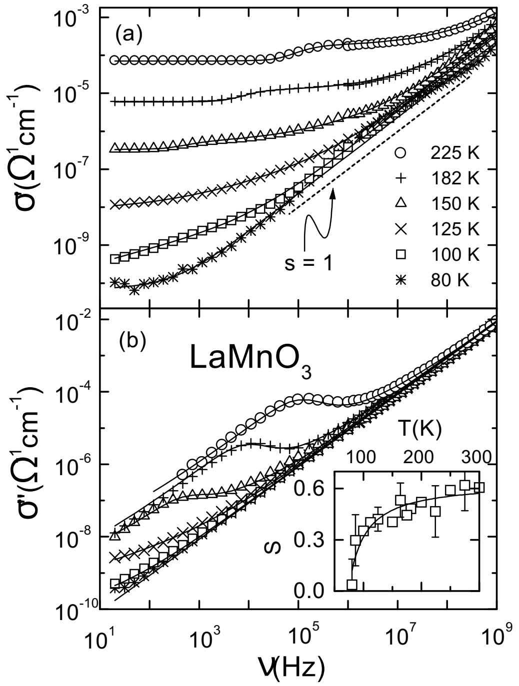

Figure 5. Frequency dependence of the real (a) and imaginary part (b) of the conductivity for $x = 0$ at various temperatures. The solid lines are fits using the equivalent circuit shown in figure 3. The dashed line indicates SU behaviour $\sigma' \sim \nu$. The inset shows the exponent parameter, s, as deduced from the fits. The line in the inset has been calculated using the SPT model [16].

as intrinsic sample response. Depending on the observed features in the spectra at different temperatures not all elements of the equivalent circuit were necessary. Apart from the relaxation

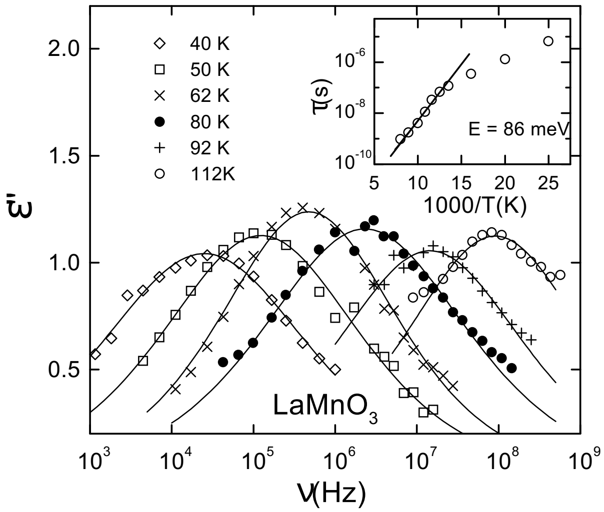

Figure 6. Dielectric loss, ε'', against frequency for $x = 0$ at various temperatures. Only data points dominated by the relaxation response are shown. The lines are fits with the Cole–Cole function [26]. The inset shows the relaxation time, τ, resulting from the fits in Arrhenius representation. At high temperature an energy barrier of $E = 86$ meV was deduced.

contribution, a good description of the data is achieved in this way giving clear evidence for the presence of hopping conductivity in a large temperature range. The inset of figure 5 shows the resulting temperature dependence of the exponent parameter s. At the highest and lowest temperatures relatively large error bars arise due to the small regions where the ν^s power law is seen unobscured from other contributions. $s(T)$ decreases with decreasing temperature and approaches zero for low temperatures (below 80 K, s could not be determined due to the dominating SU contribution). Such a behaviour is predicted by the small-polaron tunnelling (SPT) model [16]. In the SPT model, charge transport is assumed to be due to tunnelling of small polarons, `small' implying that their lattice distortions do not overlap. The line in the inset of figure 5 is a fit using the SPT prediction [16] giving a good description of the data. The resulting energy barrier $W_H = 41$ meV takes account of the fact that, besides the tunnelling motion of the electron, the accompanying transfer of the lattice deformation to the new site is thermally activated. One has to be aware that the SPT model also predicts a frequency dependence of s. Therefore equation (1) should no longer be valid in a strong sense, i.e. with s = constant. However, in the present data a `pure' ν^s contribution is seen only in relatively small frequency ranges and it can be assumed that the rather weak $\ln(\nu)$ dependence predicted for $s(\nu)$ [16] leads only to small deviations from equations (1).

Now the relaxation process will be analysed in detail. Figure 6 shows the frequency dependence of the dielectric loss $\varepsilon'' = \sigma'/(2\pi\nu\varepsilon_0)$, with ε_0 the permittivity of vacuum. Here only data points not affected by the conductivity background are shown. The relaxation shows up as a peak in $\varepsilon''(\nu)$ shifting to higher frequencies with increasing temperature. The half-width of the loss peaks is significantly broader than the 1.14 decades predicted for a monodispersive process [26]. The lines are fits with the Cole–Cole function which provides a phenomenological description of symmetrically broadened loss peaks [26]. A possible explanation for this finding is a distribution of relaxation times caused by a distribution of energy barriers for the reorientation or repositioning of the relaxing entities. The relaxation time τ resulting from the fits is plotted in the inset of figure 6 against the inverse temperature. It does not follow a thermally activated behaviour over the whole temperature range investigated. The data can be described by an Arrhenius law, $\tau = \tau_0 \exp[E/(k_B T)]$, for $T > 75$ K (line in the inset of figure 6) with deviations occurring below this temperature. The energy barrier deduced from the high-temperature thermally activated behaviour is $E = 86$ meV with $\tau_0 \approx 3 \times 10^{-13}$ s.

In this context it is interesting that in many oxide perovskites of ABO_3 type similar loss anomalies with typical energy barriers of 80 meV have been observed [27, 28]. These relaxation processes were attributed to localized hopping of polarons between lattice sites which is equivalent to the reorientation of an electric dipole [27, 28]. Evidence for the polaronic nature of the relaxation process came from the small energy barrier and the small Arrhenius prefactor $\tau_0 < 10^{-13}$ s. As the energy barrier and τ_0 of the relaxation process in $LaMnO_3$ are of similar magnitude, a polaronic origin of this feature seems reasonable. The temperature dependence of τ in the perovskites usually behaves as thermally activated in the whole temperature range but in pure [29] and doped $SrTiO_3$ [28] there is evidence for low-temperature deviations from an Arrhenius law, similar to the present results in $LaMnO_3$ (inset of figure 6). These deviations were attributed to quantum mechanical tunnelling [29] or to zero-point fluctuations (concept of `quantum polarons') [28], well known to exist in the incipient ferroelectric $SrTiO_3$ [30]. However, these processes become important in $SrTiO_3$ below 10 K only. In addition, one has to state clearly that the $\tau(T)$ data in $LaMnO_3$ may also be described assuming a second Arrhenius law below 75 K. The spectral shape of the peaks in figure 6 shows some non-trivial temperature dependence which, especially for $T \leqslant 80$ K where the conductivity background is of less importance, seems to be significant. It is interesting that there is a marked change of peak width between 62 K and 80 K just where the possible transition from tunnelling to thermally activated behaviour occurs.

Summarizing the results in $LaMnO_3$ the following picture for charge motion evolves: In the whole temperature range investigated, charge transport is dominated by hopping of Anderson-localized charge carriers. Both the results on the long-range transport and on the local relaxation mode indicate a polaronic nature of the charge carriers.

3.4. $La_{1-x}Sr_xMnO_3$, $0.05 \leqslant x \leqslant 0.125$

In the following we will give a short overview on the result for the Sr concentration range $0.5 \leqslant x \leqslant 0.125$. For $x = 0.05$ and $x = 0.075$ the overall response is similar to the one found for $x = 0$, presented in the previous section. The main difference is the absence of the SU contribution which leaves the ν^s power law as the dominating feature at high frequencies. The data were fitted in the same way as for $x = 0$ and the resulting exponent parameters $s(T)$ are shown in figures 7(a) and 7(b). In contrast to the $x = 0$ results, now a minimum in $s(T)$ shows up for both compositions. Such a minimum in $s(T)$ is predicted by the `overlapping large-polaron tunnelling' (OLPT) model [16]. In the OLPT model the charge carriers are assumed to be large polarons, i.e. the lattice distortion around the site of a charge carrier overlaps with the distortions on neighbouring sites. This gives rise to an energy barrier which is a function of the site separation. The lines in figures 7(a) and 7(b) are fits with the OLPT predictions. A good agreement with the data can be achieved for both data sets. The resulting energy barriers for infinite distance of the polaron sites [16] are $W_{HO} = 0.20$ ($\pm$0.03) eV and $W_{HO} = 0.13$ ($\pm$0.02) eV for $x = 0.05$ and $x = 0.075$, respectively. The change from SPT to OLPT can be rationalized considering the much higher charge density for the doped compounds (the conductivity is some decades higher) which may lead to an overlap of the lattice distortion clouds thus forming large polarons. One has to be aware that this distortion cloud is in fact the missing JT distortion at the Mn^{4+} site. A problem arising in this interpretation is the fact

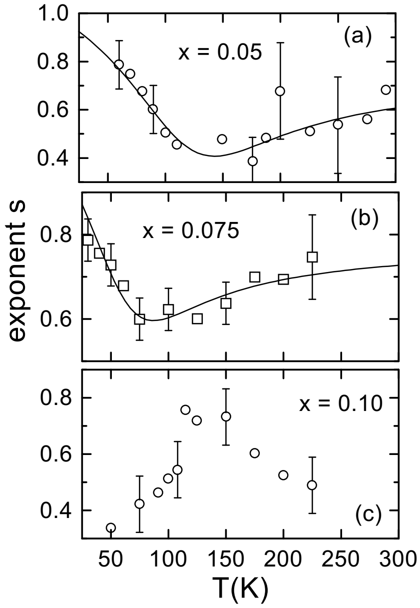

Figure 7. Temperature dependence of the exponent parameter, s, for $x = 0.05$, 0.075 and 0.1. $s(T)$ was obtained from fits of $\sigma'(T)$ and $\sigma''(T)$ using the equivalent circuit shown in figure 3. The lines in frames (a) and (b) were calculated with the OLPT predictions [16].

that the JT-generated distortion should be limited to one lattice cell only and it is questionable whether an overlap in the sense of the OLPT model can be achieved in this way.

The relaxation contribution seen for $x = 0$ is also present for $x = 0.05$ and 0.075. Similar to the results for $x = 0$, for $x = 0.05$ an energy barrier of about 90 meV and indications of low temperature deviations from thermally activated behaviour were found. For $x = 0.075$ the conductivity background was too strong to allow for a detailed analysis. The transitions into an antiferromagnetic or spin-canted state, reported for these compounds [2, 6–10], have no influence on the ac conductivity. However, a small anomaly is seen in the dc conductivity for $x = 0.05$ at 120 K (figure 1) which we attribute to this transition.

For $x = 0.1$ evidence for hopping conductivity with the characteristic ν^s contribution is also found, but at temperatures near room temperature it seems to be absent. The frequency exponent $s(T)$ (figure 7(c)) now shows a qualitatively different behaviour which cannot be explained by either the SPT or the OLPT model. For this composition a ferromagnetic transition at $T_c \approx 150$ K is assumed in most phase diagrams [6–10]. Within this picture, the anomaly in the dc conductivity at T_c (figure 1) is due to the close coupling of transport and magnetic properties in the DE mechanism (for an alternative explanation, see [31]). Another anomaly in σ_{DC} occurs at a somewhat lower temperature $T_{C2} \approx 110$ K. A recent detailed investigation of magnetic properties in the $La_{1-x}Sr_xMnO_3$ system [31] suggests a magnetic origin for this transition, too. The $s(T)$ behaviour for $x = 0.1$ (figure 7(c)) indicates an influence of these transitions on the ac conductivity: In the region between T_{C2} and T_c, $s(T)$ assumes rather high values of about 0.75 while $s \approx 0.5$ outside this region. The temperature dependence of the ac conductivity (not shown) has a change of slope near T_c. At T_{C2} a smeared-out jump in $\sigma'(T)$ is seen with a hysteresis between heating and cooling. A closer inspection reveals that this jump is split into two successive jumps, separated by about 5 K. A similar feature shows up in the dc resistivity (figure 1). A possible explanation is the succession of a structural and a magnetic transition. A more detailed treatment will be given in a forthcoming publication [31]. Relaxation contributions are absent for all concentrations $x \geqslant 0.1$.

In $La_{0.875}Sr_{0.125}MnO_3$ evidence for hopping conductivity is found for $T < 80$ K only. Due to the small frequency range where `pure' ν^s behaviour is seen, a detailed analysis of $s(T)$ is not possible. The overall response is similar to that found for $x = 0.15$ which will be discussed in detail in the following section.

3.5. *$La_{0.85}Sr_{0.15}MnO_3$*

Figure 8 shows the real part of the complex resistivity $\rho'(T)$ in $La_{0.85}Sr_{0.15}MnO_3$ at various temperatures together with the dc resistivity obtained in the four-point technique. In contrast to σ shown in figure 4 we now switch to the ρ-representation which is better suited for this rather well conducting material (see section 3.2). The imaginary part ρ'' is dominated by inductive contributions ($\sim\nu L$, L the inductance) mainly arising from the sample holder and therefore in the following only ρ' will be considered. At $T_C \approx 240$ K, the dc conductivity changes from semiconducting to metallic behaviour. According to the published phase diagrams [6–10], at this temperature a ferromagnetic phase transition occurs. Similar to $x = 0.1$ and $x = 0.125$, at a somewhat lower temperature $T_{C2} \approx 190$ K, $\rho_{DC}(T)$ recovers semiconducting behaviour which recently has been attributed to a transition into a so-called `polaron-ordered' state [9]. For $T > 40$ K, the ac resistivity curves are located above the dc curve. At temperatures $T > T_C$ the 1.8 GHz curve coincides with the dc curve. In this temperature region the enhancement of the ac resistivity at lower frequencies can be completely attributed to contact contributions which at 1.8 GHz are bridged by the contact capacitance. Between about 70 K and T_c, even at 1.8 GHz the ac resistivity is higher than ρ_{dc}. This can be explained by the skin effect (see section 3.2). At $T > T_c$, even for the highest frequencies investigated, the skin depth $\delta \sim [\rho_{dc}/(\mu\nu)]^{1/2}$ is larger or at least of similar magnitude as the sample thickness leading to no significant frequency dependence. But when the material becomes magnetically ordered, the skin effect gains importance: the magnetic ordering below T_c leads to an enhancement of the magnetic permeability μ thereby reducing the skin depth to a value smaller than the sample thickness. The resulting reduction of the effective cross section of the sample leads to the observed apparent enhancement of the ac resistivity. At the highest frequencies the measured resistance can be identified with the surface resistance, R_s, of the sample. For the surface resistance a behaviour $R_s \sim \nu^{1/2}$ is expected, and indeed for the highest frequencies, $\nu \geqslant 1$ GHz, a slight increase of $R(\nu)$ is observed (not shown). However, a quantitative evaluation is not possible as the results may be still obscured to some extent by the contact contributions and the precision of the experimental set-up is not very high in this high-frequency region. From the enhancement of the resistivity at 1.8 GHz compared to the dc resistivity, in principle the permeability can be deduced if the skin-effect-induced frequency dependence of the resistance is known. Corresponding formulae can be found in textbooks on electrodynamics but, however, for conductors with circular cross-section only. The $\mu(T)$ obtained in this way is plotted in the inset of figure 8 which can give a crude estimate of the qualitative behaviour only. At T_c, $\mu(T)$ starts to increase rapidly and near T_{C2} a pronounced peak shows up. This roughly agrees with the findings from recent magnetic measurements that provide clear evidence for the presence of two magnetic transitions at T_c and T_{C2} [31]. These transitions directly show up as two anomalies in $\rho'(T)$ at high frequencies (figure 8). At temperatures below 70 K the dc resistivity increases steeply and, due to the increased skin depth, the skin effect no longer affects the measured ac resistance.

Although the above explanation of the discrepancy of the dc and 1.8 GHz curves seems most reasonable also alternative explanations are possible. E.g., a frequency dependence of

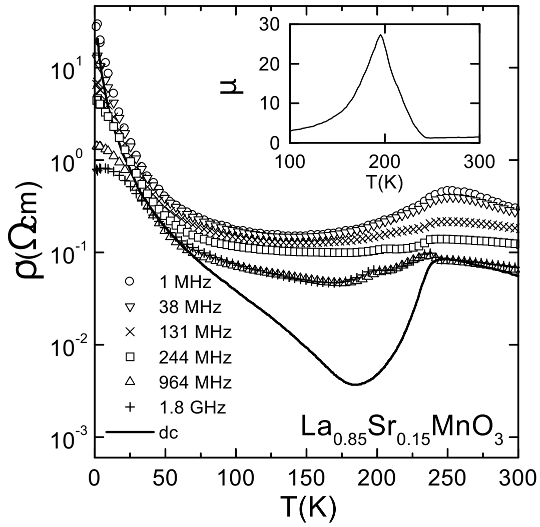

Figure 8. Temperature-dependent real part of the resistivity, $\rho' = RA/d$, for $x = 0.15$ at various frequencies. In addition, the dc resistivity is shown as a line. The inset presents the magnetic permeability, μ, calculated in the skin-effect-dominated regime from the dc and 1.8 GHz curves (see text).

the magnetic permeability cannot be excluded. In this context it is of interest that Lofland *et al* [32] in a series of publications have found a frequency-dependent μ in CMR materials due to ferromagnetic resonance effects at frequencies as low as 2.86 GHz. In addition, also an intrinsic frequency dependence of the resistivity could provide an explanation for the results of figure 8. Indeed recent transmission measurements performed in our group in the submillimetre wavelength range, which are not influenced by the skin effect, led to resistivity values similar to those reported in figure 8 [33]. A possible explanation would be a Drude-like decrease of the conductivity that may occur already below 1 GHz, but this presumption would imply unreasonably high effective masses of the charge carriers.

In the range 40 K $< T <$ 300 K the frequency-dependent sample response can be described without employing a ν^s contribution. This is demonstrated in figure 9 where the frequency-dependent resistivity is shown for four temperatures. The curves at 300 K and 50 K can well be described assuming a parallel R_c-circuit for the contact contribution in series with a frequency-independent sample resistance (dashed lines). We conclude that Anderson localization of charge carriers plays no important role for $T >$ 40 K and alternative explanations for the semiconducting behaviour in this temperature region have to be considered. In order to clarify this question we have started an investigation of the optical conductivity in $La_{1-x}Sr_xMnO_3$ [34]. First results suggest a band semiconductor picture for $La_{0.85}Sr_{0.15}MnO_3$ in this temperature range similar to the findings of Okimoto *et al* [35] for $x = 0.1$.

The finding that, at $T <$ 40 K and high frequencies, ρ' in figure 8 is lower than the dc value and decreases with frequency indicates that hopping of Anderson-localized charge carriers finally becomes important for low temperatures. Indeed the equivalent circuit used for the higher temperatures no longer works for the $\rho(\nu)$ curves at 25 K and 1.5 K (dashed lines, figure 9). These curves can be much better fitted using equations (1) (solid lines) the contacts playing only a minor role in this temperature region. The inset of figure 9 shows the

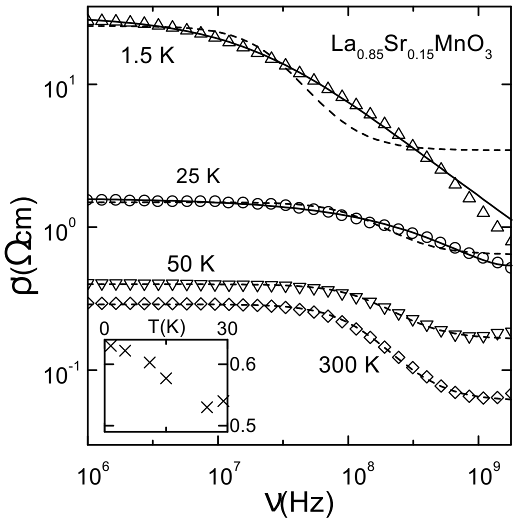

Figure 9. Frequency dependence of ρ' for $x = 0.15$ at various temperatures. The dashed lines are fits with an equivalent circuit similar to that depicted in figure 3, but with a frequency-independent sample resistance. The solid lines are fits using the UDR, equations (1), with $\rho' = \sigma'/(\sigma'^2 + \sigma''^2)$. The inset shows the temperature dependence of the frequency exponents.

temperature dependence of s. Due to the small temperature range a significant comparison with model predictions is not possible.

3.6. $La_{0.825}Sr_{0.175}MnO_3$

The temperature dependence of ρ' of $\mathrm{La_{0.825}Sr_{0.175}MnO_3}$ is presented in figure 10 for various frequencies. Due to the more metallic character of this material the contact resistance is relatively small, thus enabling the use of the four-point technique up to 1 MHz (see section 3.2). The 240 Hz curve in figure 10 resembles the dc curves reported in the literature [8, 10]. Below $T_C \approx 280$ K, $\rho'(240\ \mathrm{Hz},\ T)$ starts to decrease steeply caused by the onset of magnetic order. This corresponds to the findings for $x = 0.15$ at $T_C \approx 240$ K. At $T_S \approx 175$ K a small anomaly shows up which is commonly attributed to a structural phase transition from rhombohedral to orthorhombic form [2, 6–10]. As can be seen in figure 10, the resistivity increases with frequency in the whole temperature range. This frequency dependence becomes much stronger below T_C. Using the same arguments as for $x = 0.15$ (preceding section) this behaviour can be attributed to an enhancement of the skin effect contribution due to the increase of μ below T_C. For $\nu \leqslant 1$ MHz the surface resistance regime with its typical $R_S \sim \nu^{1/2}$ behaviour is not yet reached. After subtraction of the dc resistance, $R(\nu)$ increases more steeply than $\nu^{1/2}$ (not shown) as expected for the transition region between the dc and surface resistance regime. For the reasons mentioned in the preceding section a quantitative evaluation of the frequency dependence from the two-point measurements at $\nu \geqslant 1$ MHz is difficult. In addition to the phase transition at T_C, the skin effect seems to be affected by the phase transition at T_S, too, as the anomaly at T_S changes sign for high frequencies. The inset in figure 10 shows the temperature dependence of μ deduced from the skin effect enhancement of the resistivity. Besides the expected increase of $\mu(T)$ at T_C, there is an anomaly at T_S, too, i.e. the structural transition has an influence on the magnetic properties. This topic will be addressed in a forthcoming paper where detailed magnetic measurements on this material will

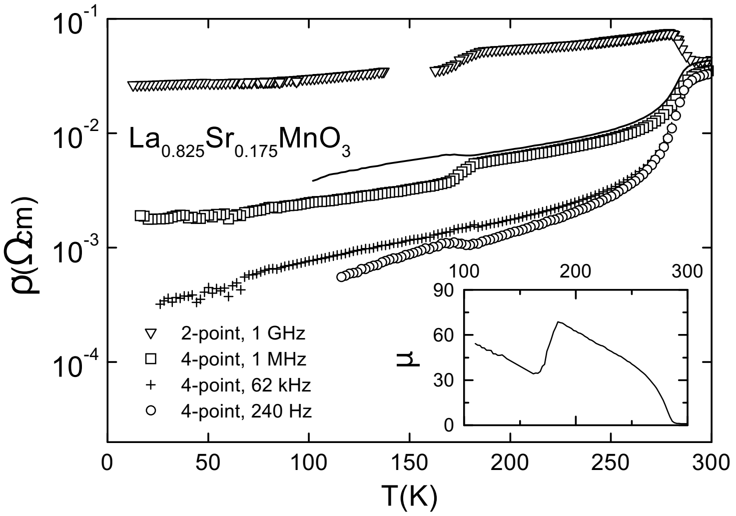

Figure 10. Temperature-dependent real part of the resistivity, $\rho' = RA/d$, for $x = 0.175$ at various frequencies. The curves have partly been obtained from four-point measurements as indicated in the legend. The inset presents the magnetic permeability, μ, calculated in the skin-effect-dominated regime from the 240 Hz and 1.8 GHz curves (see text).

be reported [31]. In the whole temperature range investigated there are no indications for Anderson localization in this compound. Similar results were obtained for $x = 0.2$.

4. Conclusions

We have investigated the dc and complex ac conductivity of the $La_{1-x}Sr_xMnO_3$ system. From the temperature-dependent ac conductivity and permeability, obtained from an analysis of the skin effect at $x \geqslant 0.15$, phase transition temperatures have been deduced which are shown in figure 11. For $x = 0.1$, 0.125 and 0.15 we find evidence for two transitions in the range 100–250 K (circles and squares in figure 11). The transitions indicated by circles are commonly assumed to be connected with magnetic ordering (ferro- or antiferromagnetic) [2, 6–10]. For $x = 0.15$ and $x = 0.175$ this is corroborated by our results in the skin-effect-dominated regime. The transitions indicated by squares can be connected with the charge ordering observed recently in this region [9]. From the skin-effect-dominated ac conductivity for $x = 0.15$ we infer a magnetic nature for this transition, too. In addition, the phase transition found for $x = 0.1$ at about 110 K is split into two transitions divided by about 5 K (open and closed square). The triangle marks the anomaly observed in the dc and ac conductivity of the $x = 0.175$ sample which is ascribed to the rhombohedral–orthorhombic transition. The additional structural phase transition reported in $La_{1-x}Sr_xMnO_3$ between the orthorhombic O and O′ phases [6–10] is not addressed in this phase diagram. The anomaly observed near 270 K for $x = 0.125$ (figure 1) which was earlier ascribed to phase separation [7] most probably is due to this transition [6, 10]. Overall, it is difficult to deduce the exact nature of the observed phase transitions from the ac conductivity measurements alone and a more detailed examination of the phase diagram including magnetic measurements will be given in a forthcoming paper [31].

The most important result of the present work is the clear evidence for hopping conductivity of Anderson-localized charge carriers in certain composition and temperature

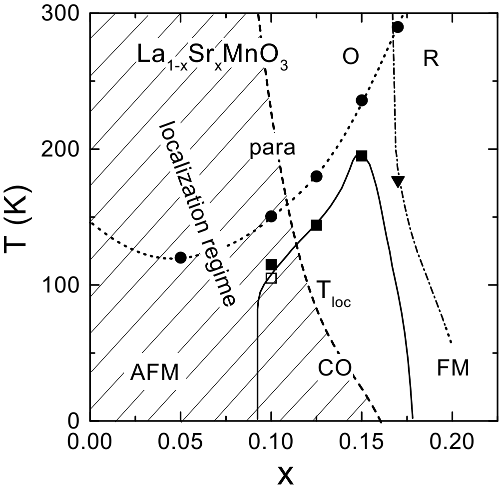

Figure 11. Phase diagram showing the localization regime (hatched area) where UDR behaviour was found, typical for hopping of Anderson-localized charge carriers. The shown phase transition points were determined from anomalies of the dc and ac conductivity and from the magnetic permeability calculated in the skin-effect-dominated regime of $\sigma(\nu)$. The lines are possible phase boundaries including information from the literature [2, 6–9]. Paramagnetic behaviour is denoted as \`para'. The transitions indicated by circles are commonly assumed to be connected with magnetic ordering (antiferromagnetic (AFM) for low and ferromagnetic (FM) for high concentrations) [2, 6–9]. The exact transition between AFM and FM regions and the role of canted spin formation is still a matter of controversy and is not addressed in this phase diagram. The squares most probably indicate a transition into a charge ordered (CO) state, recently observed in this region [9]. At $x = 0.1$ this transition is split into two successive transitions. For $x = 0.15$ we find evidence for a change of magnetic properties at this transition. The triangle lies on the border line between the rhombohedral and orthorhombic O phase. The O–O′ transition is not shown. A more detailed investigation of the phase diagram, including magnetic measurements will be given in a future publication [31].

ranges. Usually the DE mechanism with the addition of a strong electron–phonon coupling due to the Jahn–Teller (JT) effect is held responsible for the semiconducting regions of the phase diagram. This implies a band-semiconductor picture similar to a Mott–Hubbard insulator. Our results show that in certain regions of the phase diagram also Anderson localization has to be invoked in order to describe the experimental results. This \`Anderson localization regime' is shown in the phase diagram of figure 11 as the hatched area. For $x \geqslant 0.175$ Anderson localization plays no role in the transport properties of this system. For lower concentrations it becomes important for temperatures $T < T_{loc}$. This transition temperature increases with decreasing T and for $x \leqslant 0.075$, hopping prevails up to room temperature. It has to be noted that the localization regime does *not* coincide with the semiconducting regions of the phase diagram. This is demonstrated in figure 1 where the Anderson localization regime is indicated as the hatched area. Especially, it can almost certainly be excluded that Anderson localization prevails for temperatures $T > T_c$ as was suggested in recent theoretical investigations [15].

From an analysis of the frequency dependence of the conductivity within the localization regime we obtain indications for polarons as dominant charge carriers for $x \leqslant 0.075$. For higher concentrations a comparison with model predictions is difficult. It has to be stated that, also for the low concentrations, the success of the polaron hopping models used to describe the data should not be overestimated. Certainly in these materials the charge transport is more complicated than assumed in these relatively simple models which, e.g., do not take account of the DE mechanism or charge ordering. Future theoretical work in this direction would be desirable. In addition, for $x \leqslant 0.1$ a relaxation process is found resembling the relaxation processes observed in other oxide perovskites that have been attributed to a local polaronic motion [27, 28].

Overall, the results of the present investigation show that Anderson localization plays an important role in the transport properties of the perovskite manganite $La_{1-x}Sr_xMnO_3$. The very large resistivities (in comparison to the pure metallic regions of the phase diagram) observed at low doping levels and low temperatures (figure 1) are due to Anderson localization of, most probably, polaronic charge carriers. However, the MI transitions (i.e. a change of slope of the $\rho(T)$ curves) observed in certain temperature and concentration regions are not due to Anderson localization. A band-semiconductor picture, presumably of Mott–Hubbard type (driven by the DE), or the decrease of spin-disorder scattering below T_c [15] seems to be more appropriate to explain this phenomenon.

Acknowledgment

This work was supported by the BUBF, contract No 13N6917.

References

[1] Jonker G H and van Santen J H 1950 *Physica* **16** 337
Van Santen J H and Jonker G H 1950 *Physica* **16** 599
[2] For a review, see Ramirez A P 1997 *J. Phys.: Condens. Matter* **9** 8171
Von Helmolt R, Wecker J, Samwer K and Bärner K 1995 *J. Magn. Magn. Mater.* **151** 411
[3] Zener C 1951 *Phys. Rev.* **81** 440
Zener C 1951 *Phys. Rev.* **82** 403
Anderson P W and Hasegawa H 1955 *Phys. Rev.* **100** 675
DeGennes P-G 1960 *Phys. Rev.* **118** 141
[4] For a review, see: Anderson H U 1992 *Solid State Ion.* **52** 33
Minh N Q 1993 *J. Am. Ceram. Soc.* **76** 563
[5] Chahara K, Ohno T, Kasai M and Kozono Y 1993 *Appl. Phys. Lett.* **63** 1990
von Helmolt R, Wecker J, Holzapfel B, Schultz L and Samwer K 1993 *Phys. Rev. Lett.* **71** 2331
Jin S, Tiefel T H, McCormac M, Fastnacht R A, Ramesh R and Chen L H 1994 *Science* **264** 413
[6] Kawano H, Kajimoto R, Kubota M and Yoshizawa H 1996 *Phys. Rev.* B **53** R14 709
Tokura Y, Tomioka Y, Kuwahara H, Asamitsu A, Moritomo Y and Kasai M 1996 *J. Appl. Phys.* **79** 5288
[7] Zhou J-S, Goodenough J B, Asamitsu A and Tokura Y 1997 *Phys. Rev. Lett.* **79** 3234
[8] Urushibara A, Moritomo Y, Arima T, Asamitsu A, Kido G and Tokura Y 1995 *Phys. Rev.* B **51** 14 103
Moritomo Y, Asamitsu A and Tokura Y 1997 *Phys. Rev.* B **56** 12 190
[9] Yamada Y, Hino O, Nohdo S, Kanao R, Inami T and Katano S 1996 *Phys. Rev. Lett.* **77** 904
[10] Mukhin A A, Ivanov V Yu, Travkin V D, Lebedev S P, Pimenov A, Loidl A and Balbashov A M 1999 *J. Magn. Magn. Mater.* submitted
[11] Millis A J, Littlewood P B and Shraiman B I 1995 *Phys. Rev. Lett.* **74** 5144
[12] Zhao G-M, Conder K, Keller H and Müller K A 1996 *Nature (London)* **381** 676
Shengelaya A, Zhao G-M, Keller H and Müller K A 1996 *Phys. Rev. Lett.* **77** 5296
Palstra T T M, Ramirez A P, Cheong S-W, Zegarski B R, Schiffer P and Zaanen J 1997 *Phys. Rev.* B **56** 5104
Hundley M F, Hawley M, Heffner R H, Jia Q X, Neumeier J J, Tesmer J, Thompson J D and Wu X D 1995 *Appl. Phys. Lett.* **67** 860
Jaime M, Salamon M B, Pettit K, Rubinstein M, Treece R E, Horwitz J S and Chrisey D B 1996 *Appl. Phys. Lett.* **68** 1576
[13] Ju H L, Sohn H-C and Krishnan K M 1997 *Phys. Rev. Lett.* **79** 3230
[14] Zaanen G A, Sawatzky G A and Allen J W 1985 *Phys. Rev. Lett.* **55** 418
[15] Varma C M 1996 *Phys. Rev.* B **54** 7328
Sheng L, Xing D Y, Sheng D N and Ting C S 1997 *Phys. Rev. Lett.* **79** 1710
[16] Elliott S R 1987 *Adv. Phys.* **36** 135
Long A R 1982 *Adv. Phys.* **31** 553

[17] Böhmer R, Maglione M, Lunkenheimer P and Loidl A 1989 *J. Appl. Phys.* **65** 901

[18] Coey J M D, Viret M, Ranno L and Ounadjela K 1995 *Phys. Rev. Lett.* **75** 3910
Fontcuberta J, Martinéz B, Seffar A, Piñol S, García-Muñoz J L and Obradors X 1996 *Phys. Rev. Lett.* **76** 1122

[19] Mott N F and Davies E A 1979 *Electronic Processes in Non-Crystalline Materials* (Oxford: Oxford University Press)

[20] Shante V K, Varma C M and Bloch A N 1973 *Phys. Rev.* B **8** 4885

[21] Efros A L and Shklovskii B I 1975 *J. Phys. C: Solid State Phys.* **8** L49
Shklovskii B I and Efros A L 1984 *Electronic Properties of Doped Semiconductors* (Berlin: Springer)

[22] Yunoki S, Hu J, Malvezzi A L, Moreo A, Furukawa N and Dagotto E 1998 *Phys. Rev. Lett.* **80** 845

[23] Mott N F 1990 *Metal–Insulator Transitions* (London: Taylor and Francis) p 54

[24] Jonscher A K 1983 *Dielectric Relaxation in Solids* (London: Chelsea Dielectrics)

[25] Lee W K, Liu J F and Novick A S 1991 *Phys. Rev. Lett.* **67** 1559
Novick A S, Vaysleyb A V and Lim B S 1994 *J. Appl. Phys.* **76** 4429

[26] Böttcher C J F and Bordewijk P 1978 *Theory of Electric Polarization* vol II (Amsterdam: Elsevier)

[27] Bidault O, Maglione M, Actis M, Kchikech M and Salce B 1995 *Phys. Rev.* B **52** 4191

[28] Maglione M 1996 *Ferroelectrics* **176** 1

[29] Viana R, Lunkenheimer P, Hemberger J, Böhmer R and Loidl A 1994 *Phys. Rev.* B **50** 601

[30] Müller K A and Burkard H 1979 *Phys. Rev.* B **19** 3593

[31] Paraskevopoulos M *et al* 1999 *Phys. Rev. Lett.* submitted

[32] Lofland S E, Bhagat S M, Tyagi S D, Mukovskii Y M, Karabashev S G and Balbashov A M 1996 *J. Appl. Phys.* **80** 3592
Lofland S E, Ray V, Kim P H, Bhagat S M, Manheimer M A and Tyagi S D 1997 *Phys. Rev.* B **55** 2749
Lofland S E, Kim P H, Dahiroc P, Bhagat S M, Tyagi S D, Kwon C, Shreekala R, Ramesh R and Venkatesan T 1997 *J. Phys.: Condens. Matter* **9** 6697
Lofland S E, Ray V, Kim P H, Bhagat S M, Ghosh K, Greene R L, Karabashev S G, Shulyatev D A, Arsenov A A and Mukovskii Y 1997 *J. Phys.: Condens. Matter* **9** L633

[33] Pimenov A, Hartinger Ch, Loidl A, Mukhin A A, Ivanov V Yu and Balbashov A M 1998 *Phys. Rev.* B at press

[34] Mayr F *et al* 1999 to be published

[35] Okimoto Y, Katsufuji T, Ishikawa T, Arima T and Tokura Y 1997 *Phys. Rev.* B **55** 4206